Effects of grass leaf length and development stage on the triple oxygen isotope signature of leaf water and phytoliths: insights for a proxy of continental atmospheric humidity

Anne Alexandre[1], Elizabeth Webb[2], Amaelle Landais[3], Clément Piel[4], Sébastien Devidal[4], Corinne Sonzogni[1], Martine Couapel[1], Jean-Charles Mazur[1], Monique Pierre[2], Frédéric Prié[2], Christine Vallet-Coulomb[1], Jacques Roy[4].

[1]Aix Marseille Univ, CNRS, IRD, INRA, Coll France, CEREGE, Aix-en-Provence, France

[2]Department of Earth Sciences, The University of Western Ontario, London, Ontario, Canada

[3]Laboratoire des Sciences du Climat et de l'Environnement (LSCE/IPSL/CEA/CNRS/UVSQ), Gif-sur-Yvette, France

[4]Ecotron Européen de Montpellier, UPS 3248, Centre National de la Recherche Scientifique (CNRS), Campus Baillarguet, Montferrier-sur-Lez, France

Correspondance: alexandre@cerege.fr

Abstract

Continental relative humidity (RH) is a key-climate parameter but there is a lack of quantitative RH proxies suitable for climate model-data comparisons. Recently, a combination of climate chamber and natural transect calibrations laid the groundwork for examining the robustness of the triple oxygen isotope composition ($\delta^{18}O$, $\delta^{17}O$, ^{17}O-excess) of phytoliths as a new proxy for past changes in RH. However, it was recommended that besides RH, additional factors that may impact $\delta^{18}O$ and $\delta^{17}O$ of plant water and phytoliths be examined. Here, the effects of grass length, leaf development stage and day/night alternations are addressed from the growth of the grass species *F. arundinacea* in climate chambers. Plant water and phytoliths are analyzed in $\delta^{18}O$ and ^{17}O-excess. Silicification patterns are assessed. In the experimental conditions, day/night alternations do not modify the triple oxygen isotope composition of leaf phytoliths. However, additional monitoring for low RH conditions should be performed before withdrawing any generalizable conclusions. Evolution with length of ^{17}O-excess of *F. arundinacea* leaf water and phytoliths can be predicted using the Farquhar and Gan (2003) model and considering a $\lambda_{silica\text{-}water}$ value decreasing from 0.522 to 0.520 from the sheath to the apical part of the blade. Despite of this heterogeneity, the ^{17}O-excess values of bulk leaf water and phytoliths can be estimated and are not length-dependent. Overall, diversity in grass anatomy should not impact the triple oxygen isotope composition of bulk grass phytoliths. Our experiment additionally shows that as most of silica polymerizes at the end of the elongation stage (58 % in the present case), RH conditions leading to leaf senescence in nature should be considered, in addition to RH conditions during leaf elongation, when interpreting the ^{17}O-excess of phytoliths. These outcomes contribute to a more precise identification of the parameters to take into consideration when using the ^{17}O-excess of phytoliths as a proxy of RH.

1. Introduction

Recently, a combination of growth chamber and natural transect calibrations laid the groundwork for examining the robustness of the triple oxygen isotope composition of phytoliths as a new proxy for past changes in continental atmospheric relative humidity (RH) (Alexandre et al., 2018). Continental RH is a key-climate parameter. When combined with atmospheric temperature, it can be used to estimate the concentration of atmospheric water vapor, one of the main components of the global water cycle. However, global climate models have difficulties to properly capture continental RH (Sherwood et al., 2010; Risi et al., 2012; (Fischer and Knutti, 2013) and there is a lack of RH proxies suitable for model-data comparisons.

Phytoliths are micrometric particles of hydrous amorphous silica ($SiO_2(H_2O)_n$) that form in and between living plant cells. Silica polymerizes from the sap that contains dissolved silicon (among other nutrients) absorbed by the plant roots from the soil. Phytoliths, can take the shape of the cells they form in, which gives them morphological taxonomic properties. Hence, phytolith morphological assemblages extracted from buried soils, loess and sediments are commonly used for paleoenvironmental reconstructions (Miyabuchi and Sugiyama, 2015; Nogué et al., 2017; Woodburn et al., 2017). In grasses, silica that can represents several percent of the dry weight (d.w.) (Alexandre et al., 2011), polymerizes mainly in the leaf epidermis from where the plant water evaporate during transpiration (Alexandre et al., 2011; Kumar et al., 2016), and in a much lesser extent in the stem (Webb and Longstaffe, 2000). This polymerization is assumed to occur in isotope equilibrium with the plant water (Alexandre et al., 2018; Shahack-Gross et al., 1996; Webb and Longstaffe, 2000).

Variations in the triple oxygen isotope composition ($\delta^{18}O$, $\delta^{17}O$) of natural surficial waters, and consequently of minerals formed in isotope equilibrium with these waters (Gázquez et al., 2015; Herwartz et al., 2017; Passey et al., 2014) are mainly driven by the extent of kinetic fractionation during evaporation. To the contrary, they are only weakly sensitive to distillation processes (Angert et al., 2004; Barkan and Luz, 2007; Landais et al., 2008; Uemura et al., 2010; Steig et al., 2014) and not significantly affected by temperature (Barkan and Luz, 2005; Uemura et al., 2010), in contrast to variations in the deuterium-excess (d-excess = $\delta^2H - 8.0 \times \delta^{18}O$). This makes the triple oxygen isotope composition of surface waters a powerful tool for tracing evaporative conditions (Luz and Barkan, 2010)(Alexandre et al., 2018) that are mainly dependent on atmospheric RH (Cernusak et al., 2016; Craig and Gordon, 1965). In plant water, changes in the triple oxygen isotope composition due to evaporation during transpiration, can exceed most of the variations identified so far in seawater, surface water, rainfall and ice (Landais et al., 2006; Li et al., 2017; Sharp et al., 2018; Alexandre et al., 2018).

In Alexandre et al. (2018) the triple oxygen isotope composition of phytoliths from a grass species (*Festuca arundinacea*) grown under controlled conditions of RH, the other climate parameters being set constant, was examined. A linear relationship with RH was demonstrated. The triple oxygen isotope composition of soil phytoliths collected in West Africa along a vegetation and RH transect where soil water availability and climate parameters other than RH changed simultaneously, also showed a linear regression with RH, close to the correlation obtained from the growth chamber. This linear regression allowed for the prediction of RH with a standard error of 5.6%. However, it was recommended that besides RH, additional factors that may impact the isotope composition of bulk phytolith samples be examined, before using this relationship for paleoenvironmental reconstruction.

In particular, in nature, the biomass of grass stem, sheath and blade, as well as the length of leaf blade is highly species-dependant. Previous studies showed that for grasses the water $\delta^{18}O$ increases from stem to blade and from the bottom to the tip of the blade (e.g. Gan et al., 2002; Helliker and Ehleringer, 2000; Farquhar and Gan, 2003; Webb and Longstaffe, 2003; Cernusak et al., 2016). Meanwhile, the ^{17}O-excess decreases (Landais et al., 2006). This raises the question whether diversity in grass anatomy impact the ^{17}O-excess of phytoliths *vs* RH relationship.

In grasses, silica deposition can be either metabolically controlled or passive, i.e. depending mainly on silica saturation during cell dehydration when the leaf water evaporates (Kumar et al., 2017 and references therein,

Kumar et al., 2019). The contribution of evaporated water to the bulk leaf water may vary with transpiration (Cernusak et al., 2016) which changes from day to night (Caird et al., 2007) and when senescence occurs (Norton et al., 2014). This raises the question whether RH changes from day to night and from leaf elongation to leaf senescence should be considered when interpreting the the ^{17}O-excess of phytoliths as a RH proxy.

In order to address these issues, a first growth chamber experiment was set up to explore the spatial heterogeneity in $\delta^{18}O$ and $\delta^{17}O$ of water and phytoliths in *F. arundinacea.* Bulk water and phytoliths were extracted from sheaths, stems, proximal and apical leaves, young, mature and senescent bulk leaves. Silica concentration was measured and phytolith morphological assemblages, that give information on the type of tissue and cells that are silicified, were examined. A second experiment was set up to explore light/dark and day/night alternations on $\delta^{18}O$ and $\delta^{17}O$ of plant water and phytoliths of *F. arundinacea*. Implications for the calibration of the triple oxygen isotope composition of phytoliths as a RH proxy are discussed in the light of the newly acquired results.

2. The triple oxygen isotope composition of waters and minerals: notations

In the oxygen triple isotope system ($\delta^{18}O$, $\delta^{17}O$), the fractionation factors ($^{17}\alpha$ and $^{18}\alpha$) are related by the exponent θ where $^{17}\alpha = {}^{18}\alpha^{\theta}$ or $\theta = \ln{}^{17}\alpha \,/\, \ln{}^{18}\alpha$. For the silica-water couple and according to the Sharp et al. (2016) empirical equation 10, $\theta_{silica\text{-}water}$ equals 0. 524 for the 5-35°C temperature range. For the water liquid-water vapor couple at equilibrium, θ_{equil} equals 0.529 for the 11-41°C range (Barkan and Luz, 2005). When evaporation occurs, a fractionation due to the vapor diffusion in air is added to the equilibrium fractionation, as conceptualized by the Craig and Gordon model (Craig and Gordon, 1965; Gat, 1996). θ_{diff} associated with this diffusion fractionation equals 0.518 (Barkan and Luz, 2007). When RH decreases, amplitude of the diffusion fractionation governed by θ_{diff} increases. While θ applies to a particular well constrained physical process, the term λ is used when several processes occur at the same time, the resulting fractionation in the triple oxygen isotope system can be formulated as following: $\lambda = \Delta'^{17}O_{A-B} / \Delta'^{18}O_{A-B}$ with $\Delta'^{17}O_{A-B} = \delta'^{17}O_A - \delta'^{17}O_B$, $\Delta'^{18}O_{A-B} = \delta'^{18}O_A - \delta'^{18}O_B$, $\delta'^{17}O = \ln(\delta^{17}O + 1)$ and $\delta'^{18}O = \ln(\delta^{18}O + 1)$. δ and δ' notations are expressed in ‰ *vs* VSMOW. In the $\delta'^{18}O$ vs $\delta'^{17}O$ space, λ represents the slope of the line linking $\Delta'^{17}O_{A-B}$ to $\Delta'^{18}O_{A-B}$.

Another term used in hydrological studies is ^{17}O-excess ($^{17}O\text{-excess} = \delta'^{17}O - 0.528 \times \delta'^{18}O$, (Luz and Barkan, 2010) which, in the $\delta'^{17}O$ *vs* $\delta'^{18}O$ space, is the departure from a reference slope λ of 0.528. This reference slope is the trend along which meteoric waters were shown to plot (Global Meteoric Water Line expressed as $\delta'^{17}O = -0.528 \times \delta'^{18}O + 0.33$ per meg, Luz and Barkan, 2010). The average ^{17}O-excess of meteoric waters range from 35 to 41 per meg (Luz and Barkan, 2010; Sharp et al., 2018). As the reference slope is close to the liquid-vapor equilibrium exponent θ_{equil} (0.529), its use makes the ^{17}O-excess very convenient to highlight kinetic processes that result from evaporation. As the magnitudes of changes of the triple oxygen isotope composition in the water cycle and terrestrial minerals are very small, the ^{17}O-excess is expressed in per meg (per meg = 10^{-3} ‰).

3. Material

In three growth chambers, the grass species *F. arundinacea* was sown and grown in commercial potting soil in a 35 L container (53 x 35 x 22 cm LxWxD). Ten days after germination, agar-agar was spread on the soil surface around the seedlings, to prevent any evaporation from the soil as described in Alexandre et al. (2018). Ambient RH was kept constant in the growth chamber by combining a flow of dry air and an ultrasonic humidifier that produces vapor without any isotope fractionation. The vapor and the soil irrigation water (IW) came from the same source and their triple oxygen isotope composition was similar (-5.6 ± 0.0 ‰ and 26 ± 5 per meg for $\delta'^{18}O$ and ^{17}O-excess, respectively).

Experiment 1. This experiment was designed to examine the grass leaf water and phytolith isotope signatures in different parts of the leaf and at different stages of the leaf development. Briefly, the stages considered were i) young leaf, where only the end of the blade is visible as it emerges from the sheath of the preceding leaf, ii)

adult leaf where the blade is fully developed, the ligule visible and the sheath is well formed, and iii) yellow and desiccated senescent leaf.

F. arundinacea was grown for 39 days, in a climate chamber where light, air temperature and RH were set constant at 290 µmol/m^2/sec, 20°C and 73% respectively. On day 28, irrigation was stopped to force senescence of the leaves. Eleven days later, a total of 197g of biomass was collected. From this biomass, young leaf (visible end of the blade), adult leaf and senescent leaf (blade only) were separated. Adult leaves, of 24 cm length in average, were sectioned into three parts: sheath, proximal part of the blade (10 cm long) and apical part of the blade. Five samples resulted (Table 1). For all samples except the senescent leaves, three to five g of biomass were put in gastight glass vials and kept frozen for bulk leaf water extraction. Senescent leaves were too dry for water extraction. The rest of the biomass (between 10 and 70 g depending on the sample, (Table 1) was dried for phytolith extraction.

Experiment 2.a Light triggers the opening of plant stomata with, as an inevitable consequence, an increase in water loss through these stomata. At night, however, stomata often do not close totally. Night transpiration is often 5 to 15 % of day transpiration (Caird et al., 2007). In *F. arundinacea*, stomatal conductance at night can be as high as 30 % of conductance during the day (Pitcairn et al., 1986). Together with difference in air RH between day and night, this could affect isotope enrichment of leaves (Barbour et al., 2005). This experiment was thus designed to assess whether light/dark alternation may impact the isotope signature of *F. arundinacea* leaf water.

In a growth chamber, *F. arundinacea* was grown for 22 days with constant light. Then, a 12h light/12h dark alternation was introduced. Temperature and RH were kept constant at 25°C and 60% respectively. Half of the biomass was harvested at the end of day 22 (constant light). The second half was harvested at the end of the alternation period on day 26. In order to consider potential spatial heterogeneity, leaf blades (both young and adult leaves) were collected from four different places in the culture for each harvest. The eight resulting samples (Table S1) were put in gastight glass vials and kept frozen for bulk leaf blade water extraction.

Experiment 2.b In natural conditions, day/night alternations imply changes in temperature and RH in addition to changes in light intensity. This experiment was designed to assess whether over a period of several day/night alternations, changes in RH during the night impacted the mean isotope signature of grass leaf phytoliths.

For this experiment, the leaf water was not analyzed as it only gives a snapshot of its isotope composition. *F. arundinacea* was grown in two growth chambers. In the first chamber, light, temperature and RH were kept constant (290 mmol/m2/sec, 25°C and 60%, respectively). In the second chamber, 12H day/12H night alternations were set. During the day (light 290 µmol/m2/sec), temperature and RH were set to 25°C and 60%, respectively, whereas during the night (no light), they were set to 20°C and 80%, respectively. The leaf blades (both young and adult leaves) were harvested after a first growth of 16 days and a second growth of 18 days (Table S1) and dried for phytoliths extraction.

4. Methods

4.1. Phytolith chemical extraction, counting and analysis

Phytoliths were extracted using a high purity protocol with HCl, H_2SO_4, H_2O_2, HNO_3, $KClO_3$ and KOH at 70 °C following Corbineau et al. (2013) and Alexandre et al. (2018). Phytoliths were weighed and their mass reported to the initial leaf dry weight (d.w.). To account for leaf mass loss during senescence, a mass loss correction factor of 0.7, previously estimated for graminoids (Vergutz et al., 2012) was applied to the phytolith concentration in senescent leaves (Table 1a).

Most grass phytoliths have a morphology characteristic of their cell of origin. Phytolith morphological assemblages were thus determined to follow the spatial evolution over time of the leaf silicification. Phytoliths assemblages from experiment 1 were mounted on microscope slides in Canada Balsam, and counted in light microscopy at a 600X magnification. More than 200 phytoliths with a dimension greater than 5 µm and with a characteristic morphology were counted. Phytolith types were named using the International Code for Phytolith

Nomenclature 1.0 (Madella et al., 2005) and categorized as follows: Trapeziform short cell and Trapeziform sinuate short cell coming from the short cell silicification, Elongate cylindric and Elongate echinate coming from the intercoastal long cell silicification, Acicular produced by hair silicification and Parallelepipedal produced by bulliform cells silicification (Table 1, fig. 1). These characteristic phytoliths are commonly used for paleoenvironmental reconstructions when recovered from buried soils or sediments (e.g. Woodburn et al., 2017). In addition, thin silica particles with uncharacteristic shape and with a refractive index too low to be accurately described using light microscopy were also counted. Abundance of the phytolith categories are expressed in % of the sum of counted particles. Three repeated counts usually give an error lower than ± 5 % (SD).

The phytolith assemblages were further observed with a Scanning Electron Microscope (FEG-SEM, HITACHI SV6600, accelerating voltage of 3KV, 15degree tilt, working distance of 14mm and probe current of a few pA to avoid charging issues), after carbon coating.

Phytoliths triple oxygen isotope analysis was performed as described in details in Alexandre et al. (2018). The IR Laser-Heating Fluorination Technique (Alexandre et al., 2006, Crespin et al., 2008; Suavet et al., 2010) was used to extract the O_2 gas after a dehydration and dehydroxylation under a flow of N_2 (Chapligin et al., 2010). The purified O_2 gas was analysed by dual-inlet isotope ratio mass spectrometry (IRMS, ThermoQuest Finnigan Delta Plus) against a working O_2 standard calibrated against VSMOW. Each analysis consisted in two runs of eight dual inlet measurements with an integration time of 26s. The sample isotope compositions were corrected on a daily basis using a quartz laboratory standard (Boulangé). During the measurement period, Boulangé reproducibility (SD) was ± 0.13 ‰, ± 0.07 ‰ and ± 11 per meg for $\delta^{18}O$, $\delta^{17}O$ and ^{17}O-excess respectively (n = 9). For a given sample from two to three phytoliths aliquots were analyzed. Measured reproducibility ranged from 5 to 23 per meg.

4.2. Leaf water extraction and analysis

Leaf water was extracted during 6 hours using a distillation line. Then a fluorination line was used to convert water to oxygen using CoF_3. Oxygen was analyzed by dual inlet IRMS (ThermoQuest Finnigan MAT 253) against a working O_2 standard calibrated against VSMOW. The detailed procedure was previously described in Landais et al. (2006) and Alexandre et al. (2018). The reproducibility (2 replicates) was 0.015 ‰ for $\delta^{17}O$, 0.010 ‰ for $\delta^{18}O$ and 5 per meg for ^{17}O-excess.

4.3. Irrigation and vaporization water analysis

The irrigation and vaporization waters were analyzed with an isotope laser analyzer (Picarro L2140i) operated in ^{17}O-excess mode using an auto-sampler and a high precision vaporizer as described in detail in Alexandre et al. (2018). The reproducibility (3 replicates) was 0.02 ‰, 0.01 ‰ and 10 per meg for $\delta^{17}O$, $\delta^{18}O$ and ^{17}O-excess.

5. Results

5.1. Phytolith concentration, assemblage and origin in grass leaf (experiment 1)

From young to adult and senescent blade, the phytolith content increases sharply from 0.8 to 1.4 and 3.0 % d.w. This makes 58% of blade phytoliths precipitating in the late period of leaf development, at the transition between adult and senescent stages. In adult leaves, the phytolith concentration that ranges from 0.7 to 0.8% dry weight (d.w.) in sheaths and proximal blades increases to 2.1% d.w. in apical blades (Table 1). This makes half of leaf phytoliths (52% by mass) precipitating in apical blades.

Short cell phytoliths are found in all samples, while long cell phytoliths are absent from the adult sheath (fig. 1, Table S2). The ratio of long cell vs short and long cell phytoliths increases with phytolith concentration from young (29% of counted phytoliths) to adult (55% of counted phytoliths) and senescent (67% of counted phytoliths) leaf blade (fig. 2). In adult leaves, it increases from sheath (0% of counted phytoliths) to proximal (19% of counted phytoliths) and apical (59% of counted phytoliths) blade. Parallelepipedal bulliform and Acicular hair phytoliths can be observed but in small amount (<2% of counted phytoliths) in young leaves and

senescent leaf blade samples. All phytolith assemblages contain thin silica particles with low refractive index, difficult to count with accuracy in light microscopy. SEM observation shows they are composed of multi-cellular silica sheets (mostly silicified cell walls and a few silicified stomata complexes) (fig. 1). Their abundance ranges from 16 to 33% of counted phytoliths in young and adult leaf blade and increases up to 52% of counted phytoliths in senescent leaf blades (Table S2). Because these silica sheet particles are very thin, their weight contribution to the isotope signature of bulk phytolith assemblages is expected to be significantly lower than their number.

5.2. Heterogeneity in the triple oxygen isotope composition of leaf water

Irrigation and leaf water (IW and LW, respectively) $\delta'^{18}O$, $\delta'^{17}O$, and ^{17}O-excess values obtained from experiment 1 are presented in Table , Table S2 and Figure 3. As expected, the lowest $\delta'^{18}O_{LW}$ and $\delta'^{17}O_{LW}$ values occur in the adult leaf sheath which is supposed to transpire less than the leaf blade (Webb and Longstaffe, 2000, 2003). The sheath water is still ^{18}O-enriched by 7.1 ‰ relative to the irrigation water, whereas the difference in ^{17}O-excess is not significant ($^{17}O\text{-excess}_{LW\text{-}IW}$ 11 per meg). In adult leaf waters, a clear evaporative fractionation trend occurs from the sheath to the proximal and apical blade. It is expressed by a decrease in $^{17}O\text{-excess}_{LW}$ linearly correlated with an increase in $\delta'^{18}O_{LW}$ (r^2= 0.99, fig. 3). Water from the young leaf blade plots on this line, close to water from the adult upper leaf blade.

5.3. Heterogeneity in the triple oxygen isotope composition of leaf silica

When plotted in the ^{17}O-excess *vs* $\delta'^{18}O$ space (fig. 3), the phytolith from adult leaf show a clear evaporative fractionation line from the sheath to the proximal and apical blade. The young leaf blade and senescence leaf blade phytoliths plot on or slightly above this line. Given the measurement precision, young, adult and senescent leaf blades have similar $^{17}O\text{-excess}_{Phyto}$ and $\Delta'^{18}O_{Phyto}$values. $\lambda_{Phyto\text{-}LW}$ decreases from 0.522 in the sheath to 0. 521 and 0.520 in the proximal and apical parts of the blade, respectively (Table S2).

5.4. Effect of light/dark and day/night alternation on the triple oxygen isotope composition of leaf water and leaf silica.

Plant water isotope data from experiment 2a where light/dark alternations were set without changing RH, are presented in Table S1. Variations within a given set of samples (e.g. F4-02-03-17 Day or F4-02-03-17 Night in Table S1) are important, alerting that interpretation in term of kinetic *vs* equilibrium fractionation of small variations of $\Delta'^{18}O_{LW}$ (<1‰), $^{17}O\text{-excess}_{LW}$ (<14 per meg) should be avoided. When considering the margins of error, the averaged values of $\Delta'^{18}O_{LW}$ and $^{17}O\text{-excess}_{LW}$ obtained after the dark period are similar to the ones obtained after the light period. It was not possible to measure the night and day transpiration flows or the stomatal conductance during the experiment. In experiment 2b, when light/dark alternation or constant day conditions are set, differences in transpiration and leaf blade phytolith concentrations are lower than 0.1L/day and 0.2% d.w., respectively (Table S1). Differences in $\delta'^{18}O_{Phyto}$ and $^{17}O\text{-excess}_{Phyto}$ are respectively lower than 1.4‰ and 30 per meg and are not always in the same direction. In summary, under the experimental set up conditions (high RH), light/dark alternation have no obvious impact on the oxygen triple isotope composition of leaf water and phytoliths.

6. Discussion

6.1. Silicification patterns

The phytolith content and assemblages obtained from experiment 1 can be discussed in light of previous studies investigating silica deposition in grasses. In a growing grass leaf, the cells are produced at the base of the leaf and are pushed towards the tip through the elongation zone during the growth (Kavanová et al., 2006; Skinner and Nelson, 1995). Silica precipitate mainly in the epidermis. At the cell level, silicification, which is a rapid process taking a few hours (Kumar and Elbaum, 2017), initiates either in the extra-membranous space or in the cell wall and proceeds centripetally until the cell lumen is filled up (Bauer et al., 2011). During cell lumen silicification, some cells are still viable and transfer their content to each other before their full silicification (Kumar and Elbaum, 2017). Long and short cell phytoliths polymerize that way. Cell wall

silicification, not followed by cell lumen full filling, has been also frequently observed, both in the epidermis (Kumar et al., 2017) and in the bundle sheath parenchyma cells surrounding the veins (Motomura, 2004). Cell wall silicification produces the multi-cellular silica sheets observed in the phytolith samples from experiment 1. Over the course of leaf development, short cells are the first to silicify. This silicification is metabolically controlled (Kumar et al., 2017 and references therein, Kumar et al., 2019). Then, when the leaves become mature, long cell silicification takes over (Motomura, 2004; Kumar et al., 2016). In this case, silicification is supposed to be passive, i.e. its extent depends on silica saturation during cell dehydration at the evaporation sites. Passive silicification applies also to bulliform and hair cells silicification (Kumar et al., 2017 and references therein, Kumar et al., 2019). Increase of long *vs* long and short cell phytoliths from young to adult and senescent leaf blade, observed in experiment 1, confirms this pattern of silicification when leaf develops. Meanwhile, cell wall silicification, occurring throughout leaf elongation, increases drastically when the leaf reaches or is close to senescence.

Inside the adult leaf, the ratio of long *vs* long and short cell phytoliths increases from sheath to apical blade when the proportion of polymerization sites prone to evaporation increases. Meanwhile, $^{17}O\text{-excess}_{Phyto}$ decreases due to the increasing contribution of evaporated water to the bulk leaf water.

6.2. Predicted vs observed triple oxygen isotope composition of bulk leaf water

As an exercise, we estimated from experiment 1, $\delta^{18}O_{LW}$ for the bulk leaf blade water. For that purpose we used the Craig and Gordon model adapted to plant leaf water by Farquhar et al. (2007) (Table S3, adapted from spreadsheet provided in Cernusak et al., 2016). The grass transpiration was supposed to be at steady state as climatic conditions were set constant during the 39 days of growth. We also assumed that the vapor had the same isotope composition as the irrigation water since i) the vaporised water comes from the same source as the irrigation water and is not fractionated by the vaporiser, ii) there is no soil evaporation and ii) transpiration should produce a vapor with a composition similar to the one of the soil water pumped by the roots (e.g. Welp et al., 2008). We measured the temperature of adult leaf of *F. arundinacea* grown under conditions similar to those of experiment 1. No significant temperature difference was detected between the sheath, lower and upper leaf blade because the leaf temperature was probably more controlled by constant light incidence than by evaporation higher in leaf than sheath. However, the leaf was systematically 2°C cooler than the surrounding air. Thus, the model was run for 20.4 and 18.4°C. Two cases were assumed for the source water from which evaporation started: 1) water similar to irrigation water (IW in Tables S3 and S4), and 2) water similar to the measured leaf sheath water (LSW). For calculating the $\delta^{17}O_{LW}$ we used for estimating the equilibrium and kinetic fractionation (respectively $^{17}\alpha_{eq}$ and $^{17}\alpha_K$ in Table S3) $^{17}\alpha_{eq}=18\alpha_{eq}^{0.529}$ and $^{17}\alpha_k=18\ \alpha_k^{0.518}$.

For leaf temperature set at 2°C cooler than the atmospheric temperature, the predicted $\delta'^{18}O_{LW}$ and $^{17}O\text{-excess}_{LW}$ values are quasi-identical to the observed one (Table S3, Fig. 3). When leaf temperature is set similar to the atmospheric temperature the predicted $\delta'^{18}O_{LW}$ and $^{17}O\text{-excess}_{LW}$ values are respectively 2.5 to 4.5 ‰ higher and 25 to 40 per meg lower than the observed ones. This result supports that despite heterogeneity in the triple oxygen isotope composition of the water along the narrow blade, the bulk leaf blade water presents an averaged isotope signature close to the single-water-source Craig and Gordon model estimate. This result is also a reminder that, in addition to RH and the difference in the isotope signatures of tsource water and water vapor, the difference in temperature between leaf and air (which control the difference in water vapor mole fraction in the leaf air spaces and in the atmosphere, or wa/wi in Table S3) is an important parameter to consider.

6.3 Predicted vs observed triple oxygen isotope composition of water along the leaf

Along the adult leaf, evaporative fractionation appears effective as soon as the water taken up by the roots reaches the sheath where stomata are few but still present (e.g. Chaffey, 1985). This pattern was previously observed for different grass species (Webb and Longstaffe, 2003). From the sheath to the proximal and apical blade, the strong increase in $\delta'^{18}O_{LW}$, concomitant with a $^{17}O\text{-excess}_{LW}$ decrease, can be modelled using a string-of-lake approach (Gat and Bowser, 1991; Helliker and Ehleringer, 2000; Farquhar and Gan, 2003). This

approach, which implies progressively ^{18}O-enriched water segments along the leaf, is particularly adapted to the longitudinal veinal structure of grasses. Using the Farquhar and Gan (2003) equations 2, 3 and 5 and assuming a radial Péclet number of zero, as the leaf of *F. arundinacea* is narrow (<5mm), we calculated $\delta^{18}O_{LW}$ and $\delta^{17}O_{LW}$ from 0 to 24 cm length (Table S4).

Two curves can be predicted depending on the starting point of the evaporation process being the irrigation water or the sheath leaf water (fig. 3). The observed $^{17}O\text{-excess}_{LW}$ and $\delta'^{18}O_{LW}$ values in the sheath, proximal and apical blade plot closer to the predicted curve when the starting point is the sheath water. ^{18}O-enrichment of the soil water relative to the irrigation water may have occurred as previously observed for the same growth set up by Alexandre et al. (2018), due to isotope exchanges between the soil water and oxygen-bearing phases of the rhizosphere. The sheath water may reflect this modification of the soil water isotope composition. The observation that the isotope signature of the young blade plots close to the signature of the apical adult leaf blade suggests that the young leaf proximal part was not entirely sampled. Last, whatever is the length of the leaf, $\delta'^{18}O_{LW}$ and $\delta'^{17}O_{LW}$ (and consequently $^{17}O\text{-excess}_{LW}$) evolve little towards the tip where they reach their maximum values (minimum value for $^{17}O\text{-excess}_{LW}$). These $\delta'^{18}O_{LW}$ and $\delta'^{17}O_{LW}$ maxima mainly depends on the isotope enrichment of the water vapor compared to the source water, and the relative humidity with respect to the leaf temperature (Table S4 and eq. 2, 3 and 4 in Farquhar and Gan, 2003).

6.4 Predicted vs observed triple oxygen isotope composition of phytoliths

Polymerization of silica is supposed to occur in isotope equilibrium with the formation water, and, therefore, its isotope composition should only be governed by temperature and the isotope composition of the leaf water (Alexandre et al., 2018; Dodd and Sharp, 2010; Sharp et al., 2016). From the $\delta^{18}O_{LW}$, we used the thermo-dependent relationship empirically established by Dodd and Sharp (2010) to calculate $^{18}\alpha_{Phyto\text{-}LW}$ and $\delta^{18}O_{Phyto}$. Then we calculated $\alpha^{17}O_{Phyto\text{-}LW}$ using $\lambda_{silica\text{-}water}$ estimated after the empirical relationship obtained by Sharp et al. (2016, eq.10) (0.524 at 20.4°C) (Table S4). Last, two cases were assumed for the source water from which evaporation started: 1) water similar to irrigation water, (IW in Tables S3 and S4) and 2) water similar to the measured leaf sheath water (LSW in Tables S3 and S4).

In the ^{17}O-excess *vs* $\delta'^{18}O$ space, the predicted phytolith curves are above the observed data (by 50 to more than 100 per meg, figure S2). Adjusting $\lambda_{silica\text{-}water}$ to fit the data obtained for the leaf sheath and proximal leaf blade phytoliths requires a $\lambda_{silica\text{-}water}$ value of 0.522. However, even in this case, the isotope compositions of phytoliths from apical blade and bulk adult leaf plot below the modelled curves by more than 30 per meg (figure S2). Changing values for $^{18}\alpha_{Phyto\text{-}LW}$ or for leaf temperature, stomatal or boundary layer conductance, air vapor or leaf vapor pressure in the model, do not reconciliate observed and predicted isotope compositions.

The modelled curves fit better with the data when $\lambda_{Phyto\text{-}LW}$ decreases regularly from 0.522 to 0.520 from the base to the tip of the blade (fig. 3, Table S4). This implies that a kinetic fractionation may occur during silica polymerization in the epidermal cells. Its amplitude would increase from the base to the tip of the leaf. When calculating the isotope composition of phytoliths from the Craig and Gordon model leaf water estimate, and assuming a $\lambda_{Phyto\text{-}LW}$ value of 0.522, the predictions differ from the observations by 2-3 ‰ and 30-40 per meg for $\delta'^{18}O_{Phyto}$ and $^{17}O\text{-excess}_{Phyto}$ respectively. Assuming a $\lambda_{Phyto\text{-}LW}$ value of 0.521 makes the predicted $^{17}O\text{-excess}_{Phyto}$ identical to the observed one (difference of -3-8 per meg) (Fig. 3, Table S3), although $\delta'^{18}O_{Phyto}$ remains overestimated by several ‰. Almost a dozen temperature-dependent relationships have been empirically established to estimate the $\delta^{18}O$ of low temperature silica from the $\delta^{18}O$ of the forming water. Although the obtained fractionation coefficients are close (-0.2 to -0.4 ‰ $°C^{-1}$), the range of fractionation ($\Delta^{18}O$) is large (synthesis in Alexandre et al., 2012). The discrepancy between observed and modelled $\delta'^{18}O_{Phyto}$ may be attributed to this lack of accuracy in $\alpha_{Phyto\text{-}LW}$.

6.5 Tracks for assessing how day/night alternations impact the triple oxygen isotope composition of leaf water and leaf silica

The results obtained from experiments 2a show very close isotope compositions of leaf water during light and dark periods. The constancy of atmospheric relative humidity and temperature, as well as the shortness of experiment 2a (4 days with dark/light alternations after more than 2 months of constant day light) may have played against the closure of the stomata at dark. A previous study on elongating leaves of *F. arundinacea* showed that spatial distribution of water content within the elongation zone can stay almost constant during the dark and light period (Schnyder and Nelson, 1988), supporting that dark/light alternations do not always impact the stomata openness. Anyhow, a sensitivity test shows that whatever is the stomatal behavior, change in stomatal conductance does not impact significantly the Craig and Gordon $^{17}O\text{-excess}_{LW}$ and $\delta'^{18}O_{LW}$ estimates. Experiment 2b shows that under the study high RH conditions (60% during the day and 80% during the night in experiment 2b), transpiration, silicification and $^{17}O\text{-excess}_{Phyto}$ do not vary significantly from constant day to day/night conditions. However, this experiment should be completed by additional monitoring at low RH conditions before withdrawing any generalizable conclusions.

7. Conclusions for interpreting the ^{17}O-excess of grass phytolith assemblages

In nature, grass height, are highly species-dependent. Experiment 1 clearly confirmed that the $\delta'^{18}O$ and ^{17}O-excess values of leaf water evolve with leaf height. It additionally shows that the triple oxygen isotope composition of the leaf water can be modelled using a string-of-lake approach. The consequent evolution with height of the ^{17}O-excess of phytoliths can be predicted assuming a value of $\lambda_{Phyto\text{-}LW}$ decreasing from 0.522 to 0.520 from the base to the tip of the leaf. This result calls for further assessing the occurrence, extent and systematicity of a triple oxygen isotope kinetic fractionation during phytolith formation. Anyway, the ^{17}O-excess values of the bulk leaf water and phytoliths are predictable from the Craig and Gordon model and a value of $\lambda_{Phyto\text{-}LW}$ of 0.521, independently of the grass leaf height. This outcome strengthens the reliability of $^{17}O\text{-excess}_{Phyto}$ to be used as a proxy of RH. This is in line with the $^{17}O\text{-excess}_{Phyto}$ values obtained for the adult bulk blade and senescent leaf blade phytoliths (-257 and -235 per meg, respectively) being close to the values estimated from the RH-dependency of $^{17}O\text{-excess}_{Phyto}$ equation obtained in Alexandre et al. (2018) from growth chamber samples (-222 per meg) and natural transect samples (-212 per meg).

In addition to grass height, grass anatomy heterogeneity includes heterogeneity in stem *vs* leaf biomass ratio, which can change significantly with grass development stage and from a grass genus to another. Previous studies showed that phytoliths from grass stems represent less than 10 % d.w.of the overall above-ground grass silica content (e.g. Webb and Longstaffe, 2002), even in grasses with high stem biomass such as bamboos (e.g. (Ding et al., 2008). Stem phytoliths are weakly ^{18}O-enriched relatively to the soil water (Webb and Longstaffe, 2006). Thus, the contribution of stem phytoliths should slightly decrease $\delta'^{18}O_{Phyto}$ and increase $^{17}O\text{-excess}_{Phyto}$ average values. Assuming a $^{17}O\text{-excess}_{Phyto}$ difference between stem and bulk leaf of 200 per meg would lead to a $^{17}O\text{-excess}_{Phyto}$ value for stem (10 % d.w.) and leaf (90 % d.w.) phytolith assemblage higher by 20 per meg relatively to an only leaf phytolith assemblage, which is lower than the lowest reproducibility obtained when measuring 3 aliquots of phytoliths (23 per meg). Finally, neither grass height or grass anatomy should significantly impact the isotope composition of bulk grass phytoliths.

Experiment 1 gives some tracks for assessing whether senescence may impact the $^{17}O\text{-excess}_{Phyto}$ vs RH relationship calibrated for grass leaf during elongation in Alexandre et al. (2018). In the case of *F. Arundinacea,* 58% of silica polymerization occurs at the transition between the end of the elongation stage and the beginning of the senescence stage, mainly in long cells and on cell walls. Leaf senescence is a stress-induced or age-related developmental aging during which transpiration decreases to minimal level but is still efficient (Norton et al., 2014), epidermal conductance progressively prevailing over stomatal conductance (Smith et al., 2006). If the cells already contain dissolved silica, epidermal evaporation, not balanced by water input due to decreasing transpiration, may lead to silica saturation and polymerization. Isotope fractionation due to evaporation during this process should follow the Craig and Gordon model. Thus, under similar climate conditions, the isotope compositions of leaf water and phytoliths formed when senescence occurs should not be different from the isotope composition of the bulk adult leaf blade that form during leaf elongation. This is in agreement with what is observed. However, in nature, senescence occurs due to seasonal climate change

such as drastic decrease of RH in the tropical and Mediterranean areas. In these conditions, phytoliths formed during senescence may have higher $\delta'^{18}O_{Phyto}$ and lower $^{17}O\text{-excess}_{Phyto}$ values than phytoliths formed during leaf elongation. Mere monitoring of stress-induced senescence effect on $^{17}O\text{-excess}_{Phyto}$ will determine whether RH prevailing at the beginning of senescence should be considered in addition to RH prevailing during leaf elongation when interpreting $^{17}O\text{-excess}_{Phyto}$.

Overall, the data and estimates presented here contribute to a more precise identification of the parameters to take into consideration when using the $^{17}O\text{-excess}_{Phyto}$ *vs* RH relationship previously obtained (Alexandre et al., 2018). They additionally bring valuable elements to trace from phytoliths the triple oxygen isotope composition of grass leaf water, which influences the isotope signal of several processes at the soil/plant/atmosphere interface.

Acknowledgements

This study was supported by the French program INSU-LEFE and by the ANR17-CE01-0002 (HUMI-17 project). It benefited from the CNRS human and technical resources allocated to the ECOTRONS Research Infrastructures as well as from the state allocation 'Investissements d'Avenir' ANR-11-INBS-0001. We thank an anonymous reviewer for his/her valuable comment.

References

Table 1. Growth chamber experiment 1 : a) Experimental set-up, phytolith content and triple oxygen isotope data obtained for phytoliths (Phyto), leaf water (LW) and irrigation (IW).

"Adult leaves: bulk blade av." stands for the weighted average of values obtained for proximal and apical blade samples. "% d.w." stands for % dry weight. Phytolith proportion was calculated using a mass loss correction factor of 0.7 for senescent leaves (see text for explanation).

Growth conditions				Phytolith concentration			Phytoliths (Phyto)							Leaf water (LW)			
Sample	Atm. temperature	Leaf temperature	RH	Total biomass	Phyto Concentration	Phyto proportion	n	$\delta'^{18}O$	SD	$\delta'^{17}O$	SD	^{17}O-excess	SD	n	$\delta'^{18}O$	$\delta'^{17}O$	^{17}O-excess
	°C	°C	%	g	% d.w.	%*		‰		‰		per meg			‰	‰	per meg
Young leaves: blade	**20.4**	**18.4**	**73**	**57.2**	**0.8**		**3**	**38.47**	**0.17**	**20.07**	**0.21**	**-243**	**7**	**1**	**13.67**	**7.17**	**-46**
Adult leaves: sheath	20.4	18.4	73	55.6	0.8	30.4	3	34.71	0.09	18.13	0.12	-193	10	1	1.54	0.83	15
Adult leaves: proximal blade	20.4	18.4	73	35.5	0.7	17.4	3	35.60	0.12	18.59	0.14	-202	23	1	5.47	2.89	1
Adult leave: apical blade	20.4	18.4	73	35.9	2.1	52.2	2	40.76	0.02	21.25	0.02	-275	5	1	12.58	6.60	-38
Adult leaves: bulk blade av.	**20.4**	**18.4**	**73**	**71.4**	**1.4**			**39.47**	**0.14**	**20.58**	**0.17**	**-257**	**28**		**9.04**	**4.76**	**-19**
Semescent leaves: blade	**20.4**	**18.4**	**73**	**12.5**	**3.0**		**3**	**38.89**	**0.19**	**20.30**	**0.23**	**-235**	**7**				
Irrigation water (IW)															-5.59	-2.92	26

* % of bulk adult sheath and blade, ** % of the sum of counted phytoliths; ***Estimated after Dodd and Sharp, 2010; ****Estimated after eq. 12, Sharp et al., 2016

Figure 1. Growth chamber experiment 1 : SEM pictures of phytoliths from young, adult and senescent leaf blades : silicifed Trapeziform short cell (1, 2 and 3), silicified Trapeziform sinuate short cell (4), undefined silicifed short cell or broken Elongate cylindric long cell (5), silicifed Elongate cylindric long cell (6a, 6b, 7 and 8), silicifed cell wall also reported as silica sheets (9 and 10).

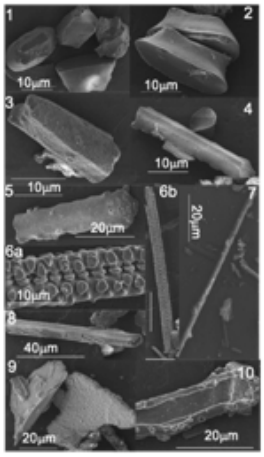

Figure 2. Growth chamber experiment 1 : a) Phytolith concentration *vs* Long Cell phytolith proportion. Error bars represent the 5% error on counting (refer to text for details).

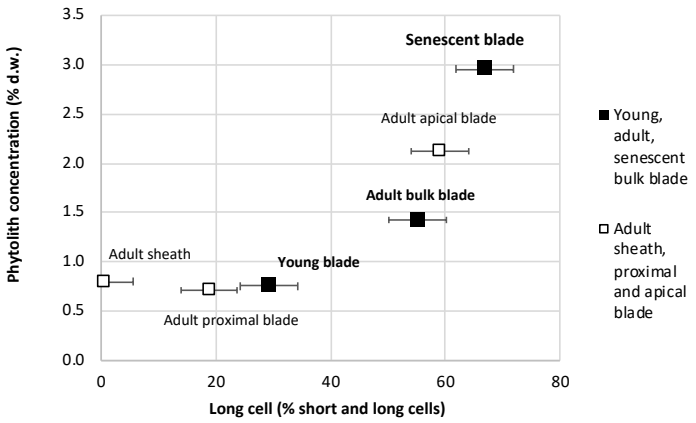

Figure 3. Growth chamber experiment 1. ^{17}O-excess *vs* δ'^{18}O observed for leaf water (LW) and phytoliths (Phyto) in young adult and senescent leaves and along adult leaf (sheath, proximal blade, apical blade).
Predicted curves depicted for leaf water along the blade according to the Farquhar and Gan (2003) model (Table S4), assuming two possiblities for the evaporation process starting point: irrigation water (IW) and leaf sheath water (LSW). Predicted curves depicted for leaf phytoliths along the blade using $^{18}\alpha_{silica\text{-}water}$ after Dodd and Sharp (2010), $^{17}\alpha_{silica\text{-}water}$ calculated from $^{17}\alpha = {}^{17}\alpha^{\lambda Phyto\text{-}LW}$ with $\lambda_{Phyto\text{-}LW}$ set for 0.522 and decreasing from 0.522 to 0.520 from base to tip (Table S4). Craig and Gordon estimates for leaf water (LW) and phytoliths (Phyto) (Table S3) assuming $\lambda_{Phyto\text{-}LW}$ of 0.522 and 0.521, and two source waters : irrigation water (IW) and sheath leaf water (SLW).

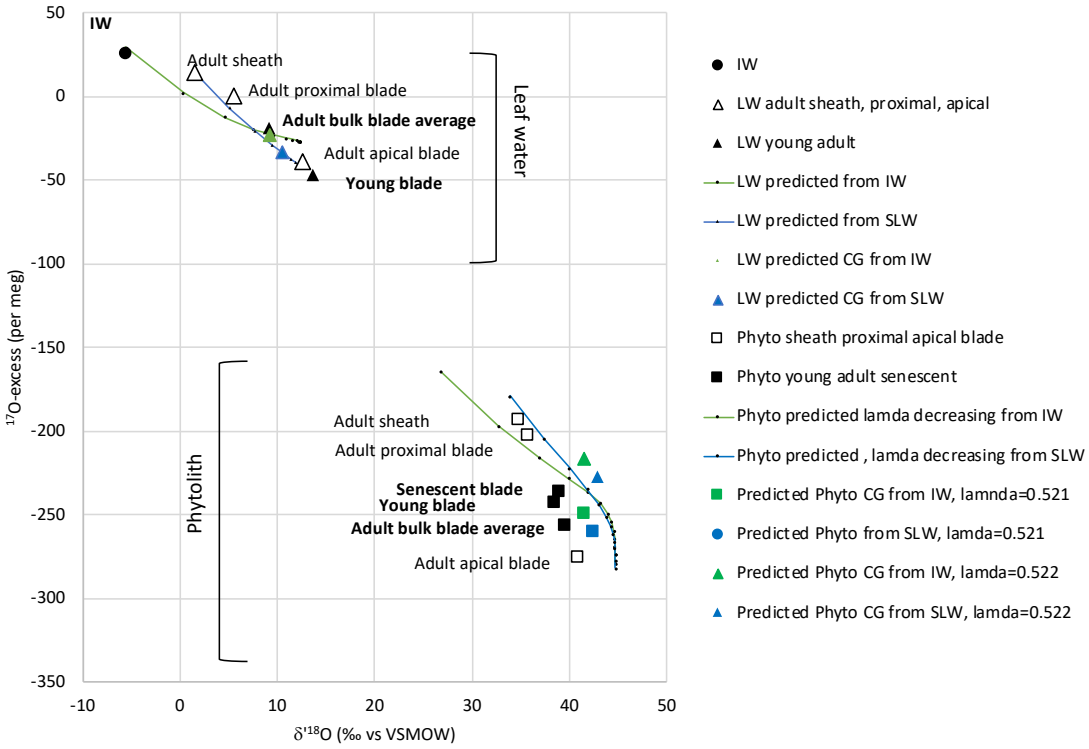

Supplementary material (cf excel file)

Table S1. Growth chamber experiment 2a and 2b. Experimental set-up, phytolith content and triple oxygen isotope data obtained for phytoliths (Phyto), leaf water (LW) and irrigation water (IW). Samples are named according to the climate chamber # they were collected in (e.g. F4), the date of sampling (dd/mm/yy) and the sampling after day or night (Day vs Night in experiment 2a) or after constant climate conditions or day/night alternation (Cst vs DN in experiment 2b). n : number of replicates ; SD : standard deviation calculated on the replicates; Phyto Conc. (% d.w.) stands for phytolith concentration expressed in % of the dry weight.

Table S2. Growth chamber experiment 1 : Experimental set-up, phytolith content, phytolith morphological assemblages and triple oxygen isotope raw data obtained for phytoliths (Phyto), leaf water (LW), irrigation (IW) and phytolith-forming water (FW). n : number of replicates ; SD : standard deviation calculated on the replicates; Phyto Conc. (% d.w.) stands for phytolith concentration expressed in % of the dry weight. "Adult leaves: bulk blade av." stands for the weighted average of values obtained for proximal and apical blade samples. "% d.w." stands for % dry weight. Phytolith proportion in senescent leaves was calculated using a mass loss correction factor of 0.7 for (see text for explanation).

Table S3. $\delta^{18}O$, $\delta^{17}O$ and ^{17}O-excess predicted for bulk leaf water (LW) and phytolith (Phyto) according to the Craig and Gordon model adapted to leaf water by Farquhar et al. (2007). After spreadsheet provided in Cernusak et al. (2016). For the water-vapor couple, the equilibrium and kinetic fractionation $^{17}\alpha_{eq}$ and $^{17}\alpha_K$ are calculated using $^{17}\alpha_{eq}=^{18}\alpha_{eq}^{0.529}$ and $^{17}\alpha_k=^{18}\alpha_k^{0.518}$. Source water is set equivalent to either irrigation water (IW) or leaf sheath water (LSW). For the silica-water couple, the fractionation factor $^{17}\alpha$ is calculated following $^{17}\alpha = ^{18}\alpha^{\lambda_{silica\text{-}water}}$ with $\lambda_{silica\text{-}water}$ set at 0.522 and 0.521.

Table S4. $\delta^{18}O$, $\delta^{17}O$ and ^{17}O-excess predicted for 1) leaf water (LW) along the blade according to the Farquhar and Gan (2003) equations 2, 3 and 5 and assuming a radial Péclet number of zero and **2) phytoliths (Phyto) along the blade using $^{18}\alpha_{silica\text{-}water}$ from Dodd and Sharp (2010), and $\lambda_{silica\text{-}water}$ equivalent to 0.522, 0.524 (Sharp et al., 2016) and ranging from 0.522 to 0.520.** See Farquhar and Gan (2003) for definition of the parameters. For the water-vapor couple, the equilibrium and kinetic fractionation $^{17}\alpha_{eq}$ and $^{17}\alpha_K$ are calculated using $^{17}\alpha_{eq}=^{18}\alpha_{eq}^{0.529}$ and $^{17}\alpha_k=^{18}\alpha_k^{0.518}$. Source water is set equivalent to either irrigation water (IW) or leaf sheath water (LSW). For the silica-water couple, the fractionation factor $^{17}\alpha$ is calculated following $^{17}\alpha = ^{18}\alpha^{\lambda silica\text{-}water}$.

Figure S1. Growth chamber experiment 1. ^{17}O-excess *vs* δ'^{18}O observed for leaf water (LW) and phytoliths (Phyto) in young adult and senescent leaves and along adult leaf (sheath, proximal blade, apical blade).

Predicted curves depicted for leaf water along the blade according to the Farquhar and Gan (2003) model (Table S4), assuming two possiblities for the evaporation process starting point: irrigation water (IW) and leaf sheath water (LSW). Predicted curves depicted for leaf phytoliths along the blade using $^{18}\alpha_{silica\text{-}water}$ after Dodd and Sharp (2010), $^{17}\alpha_{silica\text{-}water}$ calculated from $^{17}\alpha = {}^{18}\alpha^{\lambda silica\text{-}water}$ with $\lambda_{silica\text{-}water}$ set at 0.522 and 0.524 (Sharp et al., 2016). Craig and Gordon estimates for leaf water (LW) and phytoliths (Phyto) (Table S3) assuming $\lambda_{silica\text{-}water}$ of 0.522 and two source waters : irrigation water (IW) and leaf sheath water (LSW).